Modal Analysis of SPRITE Transport Processes

Frank J. Effenberger and Glenn D. Boreman

Center for Research and Education in Optics and Lasers
Department of Electrical and Computer Engineering
University of Central Florida
Orlando, FL 32816

ABSTRACT

Carrier transport in Signal Processing In The Element (SPRITE) detectors is an important phenomenon because it determines properties such as the responsivity and the modulation transfer function (MTF). The previous literature has presented approximate solutions to the transport problem that neglect boundary effects, which have long been thought to play a major role in SPRITE behavior. In this paper we present a new solution to the problem through the use of modal analysis. This method intrinsically includes the three dimensional boundary conditions, and thus is more complete than the previous analysis. Through the analysis, certain dimensionless numbers arise which can be used to characterize SPRITE structure parameters and clarify how these parameters impact device performance. Further, we use this solution to derive an expression for the MTF. The effects of the boundary conditions and the device geometry on MTF are investigated using the new theory. Our results show that the quality of the passivated surfaces has a weak influence on the MTF; however, the device width affects the MTF performance more strongly when the passivation is poor. The effect of blocking at the contacts is investigated. It is found that while marginal improvements in MTF roll-off could be achieved by making the contacts highly ohmic, the maximum signal amplitude is obtained with partially blocking contacts.

Keywords: SPRITE, infrared detectors, charge transport, MTF

1. INTRODUCTION

SPRITE detectors[1,2] provide improvement in the signal-to-noise ratio over simpler photoconductive detectors through the use of a virtual time-delay-and-integration (TDI) process internal to the detector element. The drift transport of carriers through the detector is the mechanism that makes this possible. Other transport mechanisms, such as recombination and diffusion, tend to degrade detector performance. An understanding of the interplay of these effects with the electrical boundary conditions would allow better understanding of existing devices and provide further guidance in the design and manufacture of new SPRITE detectors.

In previous analyses,[3,4,5] a one-dimensional Green's function was taken as the solution to the transport equation. This solution, which describes the charge distribution in an infinite one-dimensional solid resulting from a point source, is used as the basis of calculations to compute the transfer of a scanned incident-radiation distribution on the SPRITE detector bar into output as seen at the readout terminals.

This theory does not give complete agreement with the measurements of real devices.[6] The definition of the Green's function implicit to the analysis omits key physical phenomena in its development. The steps subsequent to the generation of the Green's function are straightforward applications of linear-systems theory, and are generally valid for this type of analysis. We have therefore used a different method, modal analysis, to solve the charge-transport equation, and developed an equivalent analysis of the transfer function of SPRITE detectors.

The method of modal analysis is more capable and requires fewer assumptions than the previous Green's function method. The first improvement is that modal analysis is multi-dimensional, whereas the Green's function method is one dimensional. While the single-dimensional approach may suffice for long, slender detector bars, most practical devices have aspect ratios that are only around 10. This fact requires consideration of the transverse dimensions. The second improvement is that the boundary conditions are included in modal analysis. The Green's function method has no boundary conditions, because of the implicit assumption of an infinite solid. The boundary conditions are important because: 1) the

0-8194-1823-4/95/$6.00

readout is usually placed at one end of the detector; and 2) most contacts made to HgCdTe have partial blocking behavior,[7] which leads to carrier accumulation at the contacts. Thus, the inclusion of boundary conditions will have a considerable impact.

Our modal solution is found by using the method of separation of variables on the transport equation, followed by determination of the eigenmodes of the separated equations.[8] This process will be shown to include the pertinent features of the system while still producing closed-form solutions. In Section 2, a more complete definition of the SPRITE transport problem will be given. Then, the modal solutions will be developed and described. After this, we will use the modal solutions to compute the impulse response, and then this will be converted into the MTF of the detector. Finally, some conclusions will be drawn about the general behavior of the MTF and the model parameters.

2. THE TRANSPORT PROBLEM

SPRITE detectors are complex devices having many features that are not easily analyzed. Among these are the details of the readout geometry, the electrical properties of the passivated surfaces, and the current-voltage characteristics of the electrical contacts. While a complete model of all these factors would require a numerical solution,[9] simplifications can be made to yield a self-consistent model that can be solved analytically and yet still contains the main features. In this section, such a mathematical description of the SPRITE transport problem will be given.

A diagram of our idealized detector is shown in Fig. 1. The detector is a rectangular solid with length, width, and depth denoted 2l, 2w, and 2d, respectively. The device has contacts on the two ends that are nominally ohmic. The top, bottom, and side surfaces are all passivated insulating boundaries. A sensing lead is placed on the bar near the output end. This lead is used to measure the voltage across the readout zone of the detector and is connected to a high-impedance amplifier.

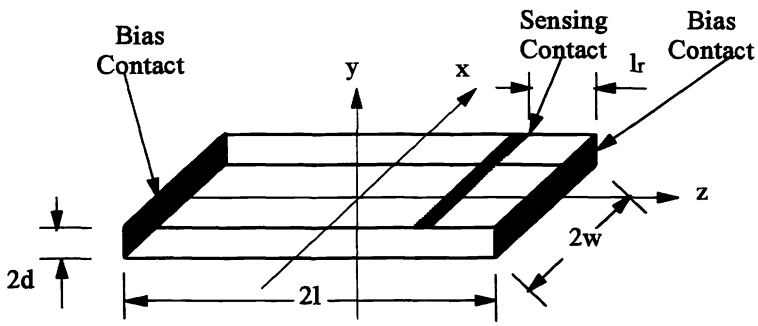

Fig. 1. SPRITE detector model geometry and coordinate system.

Operation of this detector hinges on the ambipolar drift of photon-generated minority carriers. Most HgCdTe-based SPRITEs are made of n-type semiconductor, and thus the minority holes carry the signal of interest. If the light source is scanned along the length of the bar, and the carriers drift along with it at the same speed, then the detected signal will be amplified and reinforced. This process will show the same character and advantages as a time-delay-and-integration (TDI) system, but without the necessity of separate delay-line electronics. When the intensified charge reaches the end of the detector, it causes the voltage on the sensing lead to change, thus generating a signal.

The basis for the model is the transport equation:

$$\frac{\partial \rho}{\partial t} = D\nabla^2 \rho - \mu \nabla \bullet \left(\rho E_z \hat{k}\right) - \frac{\rho}{\tau} + G \ . \tag{1}$$

This equation assumes that the carriers in the device can be described by a volumetric density, ρ, and the material can be described by a diffusivity, D; mobility, μ; and minority carrier lifetime, τ; and that there is a spatially invariant generation rate, G. These assumptions ignore the particulate nature of the charge and the resultant inherent randomness of their generation, motion, and recombination. Thus, it can be said that this equation deals with the average values for all the

quantities concerned and is deterministic. This equation also neglects the momentum of the carriers, assuming that the mean free path in the material is short compared to any other dimension of the device. This last assumption is valid in SPRITE structures because the devices are long and the electric fields are low.

The major assumption implicit in Eq. (1) is that the product of electric field and mobility, which equals the carrier-drift velocity, is assumed to be constant. This implies that the device is designed and operated in a manner that generates this condition at steady state. For simple rectangular detectors, integration of the background radiation causes this product to vary slowly over the length of the bar, with a total change of about 25%.[9] By tapering the detector bar, this nonuniformity has been reduced to insure a constant drift velocity. Also, Eq. (1) assumes that the photogenerated carriers themselves do not generate significant space-charge fields. This is true for SPRITEs because the bias current and its associated electric bias field are much stronger than the detected image signal and its field.

The boundaries of the bar, as mentioned before, are nominally either ohmic or insulating. Observations made on actual devices,[10] however, indicate behavior that differs from ideal conduction or insulation. While real surfaces are difficult to describe fully, we take the first level of complexity, which is to ascribe a surface velocity, V_s, to the passivated surfaces and to the contacts.[11] The surface velocity relates the carrier density at the surface to the carrier flux leaving through that surface according to

$$\vec{\Phi} \bullet \hat{n} = V_s \rho \,. \tag{2}$$

Carrier flux, $\vec{\Phi}$, is a vector quantity, and the normal unit vector, $\hat{n}$, is defined to be pointing out of the detector volume. The flux is caused by diffusion and drift in our model, and thus can be written as

$$\vec{\Phi} = -D\nabla\rho + \mu E_z \rho \,. \tag{3}$$

The transport equation and the six boundary conditions (one for each surface) fully describe our SPRITE transport model. This model does not ignore any feature of the detector that is vital to its operation. As will be shown in the next section, it also has a closed-form solution. These factors result in a model that is more realistic than other models previously described.

3. THE MODAL SOLUTIONS

The first step in the solution of Eq. (1) is to perform a transformation of the dependent variable to make the equation homogeneous. This discards that part of the charge distribution, equal to $G\tau$, caused by background illumination. As mentioned previously, the background charge influences detector performance in a deleterious way by making the drift velocity vary over the length; however, in all the following calculations it is assumed that steps have been taken to correct for this problem and the effect is ignored. Regardless of its spatial distribution, the background charge is constant in time. It therefore represents an unchanging offset on the signal and is of no interest as far as signal transfer is concerned. The transformation is

$$\rho = \rho' + G\tau \,. \tag{4}$$

Next, we scale all the independent variables to the natural metrics of the problem, namely the detector dimensions for the spatial coordinates and the carrier lifetime for the time:

$$x' = \frac{x}{w};\ y' = \frac{y}{d};\ z' = \frac{z}{l};\ t' = \frac{t}{\tau} \,. \tag{5}$$

The scaled coordinates are all denoted by a prime (′). Next, we employ the technique of separation of variables, which assumes that the solution for ρ' can be written as

$$\rho' = \mathrm{T}(t')\mathrm{X}(x')\mathrm{Y}(y')\mathrm{Z}(z')\exp\left(\frac{\mu E_z l}{2D} z'\right) \,. \tag{6}$$

This generates one time equation and three space equations, written:

$$\frac{\partial \mathrm{T}}{\partial t'} + k^2 \mathrm{T} = 0;\ \frac{\partial^2 \mathrm{X}}{\partial x'^2} + k_x^2 \mathrm{X} = 0;\ \frac{\partial^2 \mathrm{Y}}{\partial y'^2} + k_y^2 \mathrm{Y} = 0;\ \frac{\partial^2 \mathrm{Z}}{\partial z'^2} + k_z^2 \mathrm{Z} = 0 \,. \tag{7}$$

We have defined the time separation constant to be k^2, and the x, y, and z separation constants to be k_x^2, k_y^2, and k_z^2, respectively. These constants are related by the simple expression

$$k^2 = N_{sx}k_x^2 + N_{sy}k_y^2 + N_{sz}k_{zr}^2 + N_{dz}^2 N_{sz} + 1 \; . \tag{8}$$

We have define the dimensionless combinations of constants in Eq. (8) as follows:

$$N_{sx} = \frac{D\tau}{w^2}; \; N_{sy} = \frac{D\tau}{d^2}; \; N_{sz} = \frac{D\tau}{l^2}; \; N_{dz} = \frac{\mu E_z l}{2D} . \tag{9}$$

The constants denoted N_{sx}, N_{sy}, N_{sz} are the ratios of the carrier recombination lifetime to the carrier spatial-relaxation lifetimes, and they depend on the physical dimensions of the detector, the diffusivity, and the carrier lifetime of the material. By spatial-relaxation lifetime, we refer to the characteristic time for localized disturbances in the carrier distribution to spread because of diffusion. The magnitude of N_{sx}, N_{sy}, N_{sz} determine whether diffusion or recombination is the dominant process of carrier-distribution relaxation. The constant N_{dz} relates the lifetime of the charge distributions to the transit time of carriers in the device. It determines the degree of diffusional spreading that occurs during the time the carriers drift and accumulate in the detector.

We notice that the time equation is of first order, and has the solution

$$T(t') = \exp\left(-k^2 t'\right) . \tag{10}$$

The x, y, and z equations are second order and have general solutions:

$$X(x') = c_{xp} \cos\left(k_{xp}x' + p\,\tfrac{\pi}{2}\right); \; Y(y') = c_{yq} \cos\left(k_{yq}y' + q\,\tfrac{\pi}{2}\right); \; Z(z') = c_{zr} \cos\left(k_{zr}z' + r\,\tfrac{\pi}{2}\right) , \tag{11}$$

where p, q, and r are the serial numbers for the x, y, and z solutions, respectively.

Now that the general solutions have been written, the boundary conditions can be applied. Because the variables have been scaled and separated, the boundary conditions can be written:

$$\frac{\partial X}{\partial x'} = N_{bx} X\big|_{x'=-1}; \; \frac{\partial X}{\partial x'} = -N_{bx} X\big|_{x'=+1} \tag{12a}$$

$$\frac{\partial Y}{\partial y'} = N_{by} Y\big|_{y'=-1}; \; \frac{\partial Y}{\partial y'} = -N_{by} Y\big|_{y'=+1} \tag{12b}$$

$$\frac{\partial Z}{\partial z'} = N_{bz} Z\big|_{z'=-1}; \; \frac{\partial Z}{\partial z'} = -N_{bz} Z\big|_{z'=+1} , \tag{12c}$$

where we define three new dimensionless boundary numbers:

$$N_{bx} = \frac{V_x w}{D}; \; N_{by} = \frac{V_y d}{D}; \; N_{bz} = \frac{V_z l}{D} \; . \tag{13}$$

These constants describe the ratio of the boundary velocities with the "diffusion velocity," that is, the velocity at which diffusion spreads disturbances across the device. It provides a comparison of the speed of surface recombination with the speed of diffusion.

By substituting the general solutions into these equations, we can find the allowed values of the separation constants, thus completing the solution. This results in the following transcendental relations:

$$k_{xp} = N_{bx} \cot\left(k_{xp} + p\,\tfrac{\pi}{2}\right), \tag{14a}$$

$$k_{yq} = N_{by} \cot\left(k_{yq} + q\,\tfrac{\pi}{2}\right), \tag{14b}$$

$$k_{zr} = N_{bz} \cot\left(k_{zr} + r\,\tfrac{\pi}{2}\right) . \tag{14c}$$

Figure 2 is a graph of the first few roots any of Eqs. (14) as a function of the boundary parameter, N_{bx}, N_{by}, or N_{bz}. A series of roots results from this type of equation because the mode indices, p, q, or r, can assume all positive integer values. For small or large values of boundary parameter, the curves tend towards limiting asymptotes.

So far we have named seven independent dimensionless numbers that describe the model of the SPRITE detector. We shall now show that this is the correct number of constants needed to describe the problem as given. The model developed in Section 2 has nine independent parameters: the length, width, and depth of the detector, the surface velocities of the ends, the sides, and the faces, the diffusivity, the lifetime, and the drift velocity. In this problem, two units of measure are used, length and time. The pi theorem[12] states that the number of independent dimensionless constants needed to describe a problem is equal to the number of measured parameters less the number of units of measure. Thus for our problem, this states that seven numbers are necessary. Because the seven numbers defined here are independent from each other, they must form a sufficient, complete set of numbers completely describing the problem. To provide a feeling for the usual ranges for these numbers, typical values for these numbers have been computed using data presented in references 2, 7 and are shown in Table 1.

While our set of dimensionless numbers are complete, they do not represent the only set of numbers that could be formulated that have this property. What makes them particularly useful for our analysis is that they appear so naturally and explicitly in the differential equations and their solutions. This both eases the expression of the solutions and provides insight into the actual influence of the device parameters on device performance. This can be seen in the case of the boundary numbers.

Intuitively, the best detector will have no recombination on the sides and faces and have ohmic contacts at the ends. Any realistic fabrication process cannot achieve such surfaces, however, and thus the question is raised as to how good do the surfaces need to be. This question can be answered through use of the boundary numbers. The asymptotic behavior shown in Fig. 2 demonstrates that, for sufficiently large or small values of boundary number, no further change in the modal wavenumbers occurs. Because these wavenumbers are the only way in which the boundary conditions can affect the final solution, we can justifiably say that, for practical purposes, a boundary number below 1/100 is "insulating," and that a boundary number above 100 is "ohmic."

Parameter	Value
N_{dz}	75
N_{bx}	15×10^{-3}
N_{by}	2.5×10^{-3}
N_{bz}	3.75
N_{sx}	1.0
N_{sy}	36
N_{sz}	6.4×10^{-3}

Table 1. Typical values of detector numbers for SPRITE detectors.

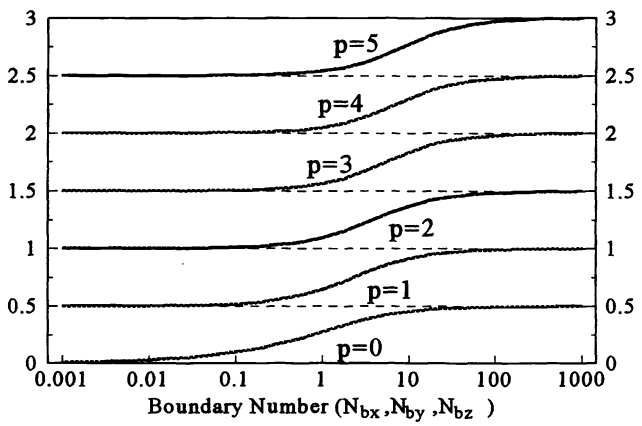

Fig. 2. Solutions to the modal wavenumbers vs. boundary number. Notice how solutions approach asymptotes.

4. MODULATION TRANSFER FUNCTION (MTF)

Now that the behavior of the individual modes of the SPRITE structure have been determined, we can derive the MTF of the detector. The MTF provides the most convenient expression of signal fidelity performance for imaging systems. Thus it is useful to compute the MTF from the physical parameters of the device. In this section, we shall derive a general form for the MTF and special cases that result in simplification. Several families of MTF curves will be computed and compared to detect trends in the general character of the MTF as a function of detector parameters.

We first define the input presented to the detector. Because the SPRITE is used as a one-dimensional detector, we shall use a one-dimensional delta function that can be scanned across the detector aperture, written as

$$q_i(z',t') = \delta(z' - z'_0), \tag{15}$$

where the scanned location, z'_0, is given by

$$z'_0 = v't' = t'/\bar{v}'. \tag{16}$$

The constants in Eq. (16), v' and $\bar{v}'$, represent the normalized scanning velocity and its inverse, respectively. Because the scan is typically matched to the drift velocity, we can write the following relation:

$$v' = \frac{\tau}{l}\mu E_z = 2\left(\frac{\mu E_z l}{2D}\right)\left(\frac{D\tau}{l^2}\right) = 2N_{dz}N_{sz} \ . \tag{17}$$

Although this input is one-dimensional, the three-dimensional nature of our solution does not necessarily vanish. When decomposed, this input will produce a three-dimensional series of modes, each having its own decay-time constant. We now decompose this input into the modes of the structure:

$$q_i = \sum_{p,q,r} c_{pqr}\, X_p(x')Y_q(y')Z_r(z')\exp(N_{dz}z'). \tag{18}$$

Because the circular-function portion of the eigenfunctions are orthogonal, we can solve for the amplitudes of the individual modes arising from the input at any particular point z'_0, giving

$$c_{pqr} = \frac{\left|\mathrm{sinc}(k_{xp})\right| \quad \left|\mathrm{sinc}(k_{yq})\right| \quad e^{-N_{dz}z'_0}\cos(k_{zr}z'_0 + r\frac{\pi}{2})}{\left[1+\left|\mathrm{sinc}(2k_{xp})\right|\right]\left[1+\left|\mathrm{sinc}(2k_{yq})\right|\right] \quad \left[1+\left|\mathrm{sinc}(2k_{zr})\right|\right]} \tag{19}$$

if p and q are even. If p or q is odd, $c_{pqr} = 0$.

These mode coefficients represent the amplitude of each mode that results from the delta-function input at the specified z' coordinate, z'_0. These amplitudes then fully specify the carrier distribution inside the detector for all time after the input. Thus these mode coefficients essentially translate the given input into a charge distribution inside the detector.

We next evaluate the output voltage resulting from a given set of modes as they decay over time. In the SPRITE, the measured output voltage is proportional to the charge in the readout region. The output resulting from charge generation located at z'_0 is thus proportional to the charge in the readout volume, Q, given by

$$Q(t',z'_0) = \sum_{pqr} c_{pqr}\, u(t' - \bar{v}'z'_0)\exp\left[-k^2_{pqr}(t' - \bar{v}'z')\right] b_{pqr} \ , \tag{20}$$

where b_{pqr} are the mode output weighting factors, given by

$$b_{pqr} = \frac{\left|\mathrm{sinc}(k_{xp})\right|\left|\mathrm{sinc}(k_{yq})\right|}{N^2_{dz} + k^2_{zr}} e^{N_{dz}} \left\{ \begin{array}{l} \left[1-\cos(k_{zr}l'_r)\right]\left[N_{dz}\cos(k_{zr}+r\frac{\pi}{2}) + k_{zr}\sin(k_{zr}+r\frac{\pi}{2})\right] \\ +\sin(k_{zr}l'_r)\left[N_{dz}\sin(k_{zr}+r\frac{\pi}{2}) + k_{zr}\cos(k_{zr}+r\frac{\pi}{2})\right] \end{array} \right\}, \tag{21}$$

if p and q are even. If p or q is odd then $b_{pqr} = 0$.

The total scanned impulse response, Θ, as a function of time, is the point impulse response, Q, integrated over the entire scan, which is to say, over the entire detector. Thus

$$\Theta(t') = \int_{-1}^{1} dz'_0 Q(t', z'_0) \ . \tag{22}$$

Because we are ultimately interested in obtaining the transform of the scanned function, $\overline{\Theta}$, we choose to take the transform now, yielding

$$\overline{\Theta}(\omega') = \int_{-1}^{1} dz'_0 \overline{Q}(\omega, z'_0) \ . \tag{23}$$

We thus need the time-domain Fourier transform of Q(t,z), which can be found to be:

$$\overline{Q}(\omega',z_0') = \Im\{Q(t',z_0')\} = \sum_{pqr} c_{pqr} b_{pqr} \frac{\exp(-j\bar{v}'\omega' z_0')}{k_{pqr}^2 + j\omega'} . \tag{24}$$

Substituting this into the integral for the total output, we can write

$$\overline{\Theta}(\omega') = \int_{-1}^{1} dz_0' \sum_{pqr} c'_{pqr} \frac{\exp(-N_{dz} - j\bar{v}'\omega')z_0'}{k_{pqr}^2 + j\omega'} \cos\left(k_{zr} z_0' + r\tfrac{\pi}{2}\right) , \tag{25}$$

where we have defined a new set of constants, c'_{pqr}, which contain all the factors independent of the position of the input, z_0'. We do this because we must integrate over this variable, and these factors will not play a role in this integration. These are defined

$$c'_{pqr} = b_{pqr} \frac{\left|\mathrm{sinc}\left(k_{xp}\right)\right| \left|\mathrm{sinc}\left(k_{yq}\right)\right|}{\left[1+\left|\mathrm{sinc}\left(2k_{xp}\right)\right|\right]\left[1+\left|\mathrm{sinc}\left(2k_{yq}\right)\right|\right]\left[1+\left|\mathrm{sinc}\left(2k_{zr}\right)\right|\right]} . \tag{26}$$

If we now integrate Eq. (25) term by term, we arrive at the final result:

$$\overline{\Theta}(\omega') = \sum_{pqr} \frac{c'_{pqr} \left\{ \begin{array}{l} \left[\exp(-N_{dz} - j\bar{v}'\omega' z') + (-1)^r \exp(N_{dz} + j\bar{v}'\omega' z')\right] \\ \times \left[k_{zr}\sin(k_{zr} + r\frac{\pi}{2}) - (N_{dz} + j\bar{v}'\omega')\cos(k_{zr} + r\frac{\pi}{2})\right] \end{array} \right\}}{\left[k_{pqr}^2 + j\omega'\right]\left[\left(N_{dz} + j\bar{v}'\omega'\right)^2 + k_{zr}^2\right]} . \tag{27}$$

This is an expression for the Fourier transform of the impulse response of a SPRITE detector as described by our model. The MTF is simply the normalized magnitude of this function, written:

$$MTF(f_z) = \left| \frac{\overline{\Theta}(2\pi l v' f_z)}{\overline{\Theta}(0)} \right| \tag{28}$$

where f_z is the spatial frequency measured in cycles per unit length (i.e., cycles/mm). It should be noted that in the graphs presented in Section 5, the frequency will be given in terms of cycles per detector length.

Because the MTF is expressed as an infinite sum, we can only compute an approximation of its value. This inaccuracy is in the computation only, and can be arbitrarily reduced through the inclusion of more terms in the series and by the use of higher-precision computation. It is important to determine the number of terms required to achieve a given level of accuracy. The x and y summations are driven to converge by the sinc^2 functional dependence of the modal weights. Our studies show that, for the typical values listed above, the x and y series converge to 0.1% in very few terms (on the order of 10). The z-series behavior can be best understood by observing the simplified case of perfect boundary conditions. The sum, whose terms alternate sign, is driven to convergence by the factors $N_{dz}^2 + \left(\frac{\pi}{2}\right)^2 (r+1)^2$ in the denominator of each term. Thus it is necessary to continue the sum until the z serial number is much larger than the drift number N_{dz}. We find that on the order of 10,000 terms are required to achieve 0.1% accuracy.

5. RESULTS AND DISCUSSION

A computer program was developed to evaluate Eq. (27) for a given set of parameters and frequencies. We used a Microsoft FORTRAN compiler running on a 486DX2/66-based desktop personal computer. Double-precision computations were used to preserve the accuracy of the sum because the sum's oscillatory behavior tends to amplify roundoff errors. MTF curves could be generated in less than ten minutes with this system, thus proving the tractability of this numerical approach.

Figure 3 is a graph of the MTF for a detector with the typical values given in Table 1, along with the curve as computed with the Green's function analysis for the same parameters in references 3, 4, and 5. Both have similar low-pass

behavior, but the modal analysis predicts a lower roll-off frequency than the Green's function analysis. This would put the modal analysis in better agreement with the measured responses of real SPRITE devices.

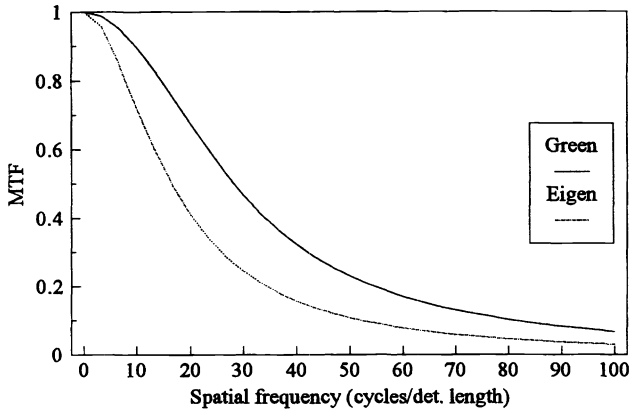

Fig. 3. Computed MTFs for Green's function method and eigenmode method.

Because the modal analysis includes the boundary conditions in the solution of the problem, we can study their effects. In Fig. 4, we have plotted MTFs of detectors having different insulating surface-recombination rates. The velocity was varied from 1/100 to 100 times the nominal value in Table 1. The resultant curves show little or no effect on the MTF until the surface recombination becomes fairly strong. Interestingly, the less insulating the sides become, the wider the MTFs become. This can be understood by considering the surface recombination as a modal-damping effect. Higher recombination makes the higher transverse modes of the device dissipate faster, and this makes the overall response faster. However, dissipation of the signal charge also reduces the absolute signal levels. This can be seen in Fig. 5, which shows the zero-frequency SiTF plotted as a function of the insulating boundary condition. The signal level is normalized to one at the nominal value of insulating boundary parameters, and it drops as these parameters are made more conductive. We can thus draw the conclusion that it is best to reduce the surface recombination, but only because it improves the signal efficiency of the detector and not because of MTF considerations.

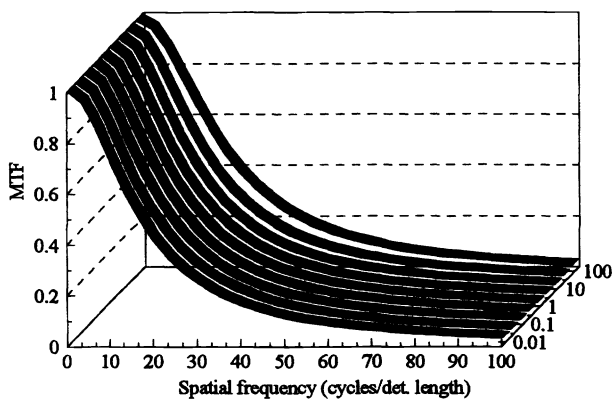

Fig. 4. MTF vs. frequency as top, bottom, and side boundary parameters are varied from 0.01 to 100 times normal value.

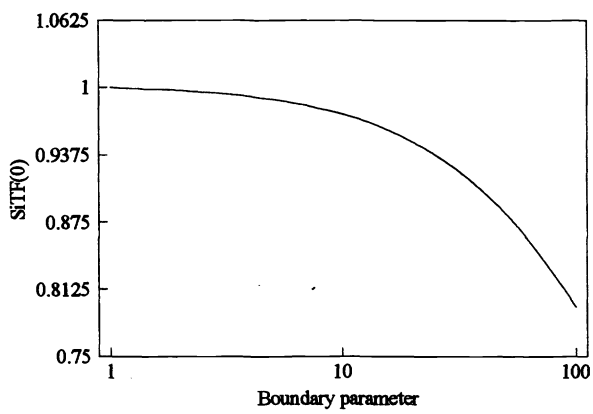

Fig. 5. Variation of the zero frequency SiTF as top, bottom, and side boundary parameters are varied from 1 to 100 times normal value.

The effect of the width of the SPRITE detector can be studied directly using modal analysis. It was found that, with the top, bottom, and side boundary parameters set to their normal values, changing the width had little effect. Because the normal values were almost totally blocking, the placement of the side boundaries (i.e., the width) would have almost no importance. When we set the side, top, and bottom boundary conditions to be fifty times their normal velocity, we obtain the data in Fig. 6, which is the MTF versus frequency as the width spreading number, N_{sx}, was varied. The MTF broadens as the width number increases, which corresponds with the actual width getting smaller because as the detector narrows, the carriers have less room to wander and blur. This gain in MTF also results in a reduction of the total signal level, as can be seen in Fig. 7, where the zero frequency SiTF function is plotted versus width spreading number. The gradual roll-off of the signal level can be seen distinctly. The conclusions one can make is the width of the detector can be important if the side boundary conditions are leaky, and if so, increasing the width increases the signal level to a certain point after which no further gains can be made. In the case of our typical detector, that point was $N_{sx} = 1$.

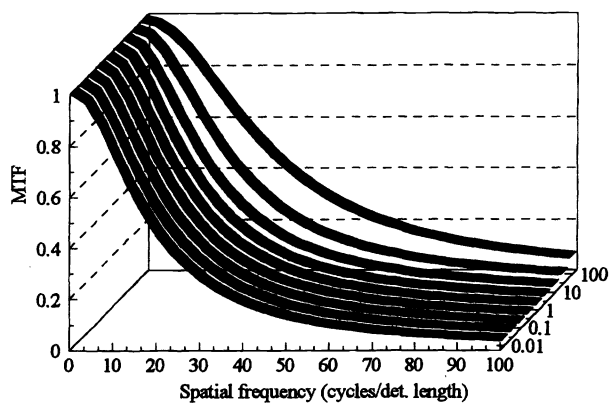

Fig. 6. MTF vs. frequency as width spreading parameter is varied from 0.01 to 100 times normal value. The side boundary conditions are 50 times normal.

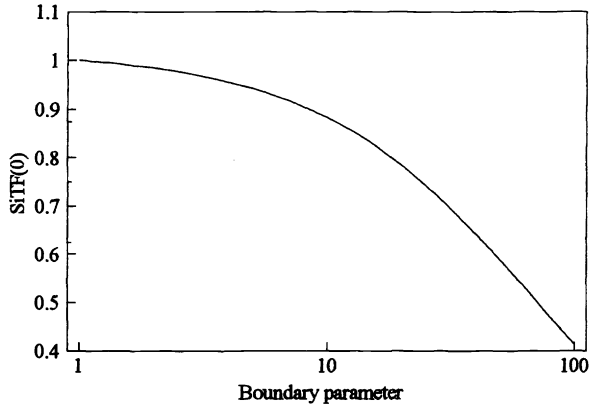

Fig. 7. Variation of the zero frequency SiTF as the width spreading parameter is varied from 1 to 100 times normal value. This corresponds to widths ranging from 1 to 1/10 normal.

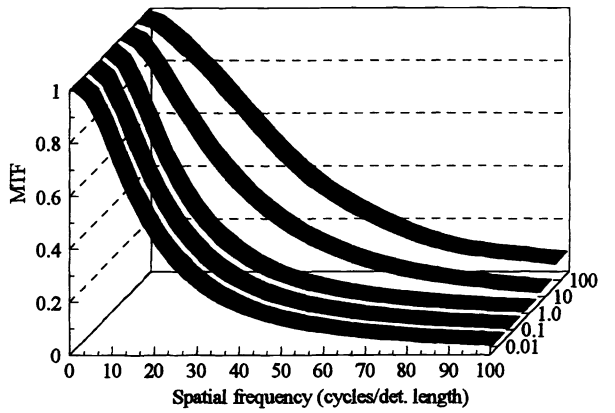

Fig. 8. MTF vs. frequency as contact boundary parameter is varied from 0.01 to 100 times normal value.

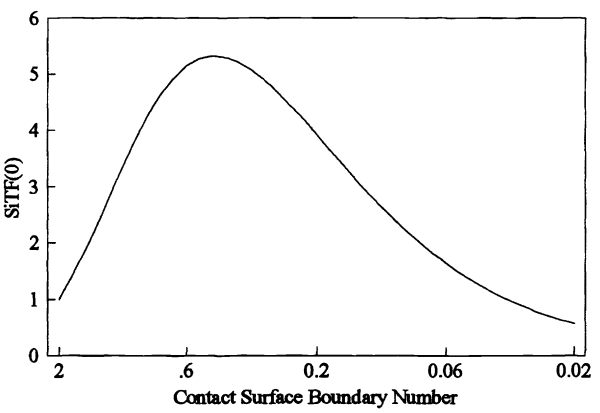

Fig. 9. Zero frequency SiTF vs. contact boundary parameter. Optimum value of parameter is around 0.5.

In Fig. 8, we have generated MTF curves for detectors having different contact recombination rates. The velocity was varied over the range of 1/100 to 100 times the nominal value. As would be expected, the higher the surface velocity, the

faster the response. This broadens the MTF curves and indicates that the contact quality has an effect on the MTF. These curves do not address the absolute signal levels, however. The zero frequency SiTF curve is shown in Fig. 9. The boundary number here varies between 1/100 to 1 times the nominal value. These graphs show that for low or high values of contact velocity, the response is reduced. This reduction is so great that it swamps the broadening of the MTF at high surface velocities. This graph clearly illustrates that the signal strength goes through a maximum when the contact boundary parameter is approximately 0.50. This corresponds to a surface recombination velocity, for our typical detector, of 40 cm/s. If possible, such tailoring of the contact velocity of SPRITE detectors could result in large increases in their signal-level performance.

5. CONCLUSIONS

In this paper we have presented a new solution to the problem of carrier-transport dynamics in SPRITE detectors through the use of eigenmodal analysis. In doing so, we developed a self-consistent model for the detector. This model and method intrinsically includes boundary conditions and full dimensionality, and thus is more complete. Through the analysis, certain dimensionless numbers arise that can be used to characterize SPRITE structure parameters and clarify how these parameters impact device performance. Expressions for the MTF have been derived, and various representative computed functions are presented. From these curves, optimum values for the insulating and contact boundary numbers have been determined.

6. ACKNOWLEDGMENT

This work was supported by Westinghouse Electric Corporation, Orlando, Florida.

7. REFERENCES

1. C. T. Elliot, US Patent #3,995,159, Nov. 30, 1976.
2. C. T. Elliot, "New detector for thermal imaging systems," Electron. Lett. **17**, 312-313 (1981).
3. D. J. Day and T. J.Shepherd, "Transport in photoconductors - I," Solid State Electronics **25**, 707-712 (1982).
4. T. J. Shepherd and D. J. Day, "Transport in photoconductors - II," Solid State Electronics **25**, 713-718 (1982).
5. G. D. Boreman and A. E. Plogstedt, "Modulation transfer function and number of equivalent elements for SPRITE detectors," Appl. Opt., **27**, 4331-4335 (1988).
6. S. P. Braim and A. P. Campbell, "TED (SPRITE) detector MTF," IEE Conf. **228**, 63-66 (1983).
7. T. Ashley, C. T. Elliot, "Accumulation effects at contacts to n - type cadmium mercury telluride photoconductors," Infrared Physics **22**, 367-376 (1982).
8. M. Boas, Mathematical Methods in the Physical Sciences, *2nd Ed.* (John Wiley and Sons, New York, 1983) p. 541.
9. T. Ashley et al. "Optimization of spatial resolution in SPRITE detectors," Infrared Physics **24**, 25-33 (1984).
10. J. A. Whitlock, G. D. Boreman, H. K. Brown, and A. E. Plogstedt, "Electrical network model for SPRITE detectors," Opt. Eng. **30**, 1784-1787 (1991).
11. S. M. Sze, *Physics of Semiconductor Devices* (Wiley Interscience, New York, 1969), p. 71.
12. E. Buckingham, Phys. Rev. **4**, 345-376 (1914).